IEEE Photonics Journal
An IEEE Photonics Society Publication

Open Access

Evaluation of a Transparent Display's Pixel Structure Regarding Subjective Quality of Diffracted See-Through Images

Volume 9, Number 4, August 2017

Zong Qin
Jing Xie
Fang-Cheng Lin
Yi-Pai Huang
Han-Ping D. Shieh, *Fellow, IEEE*

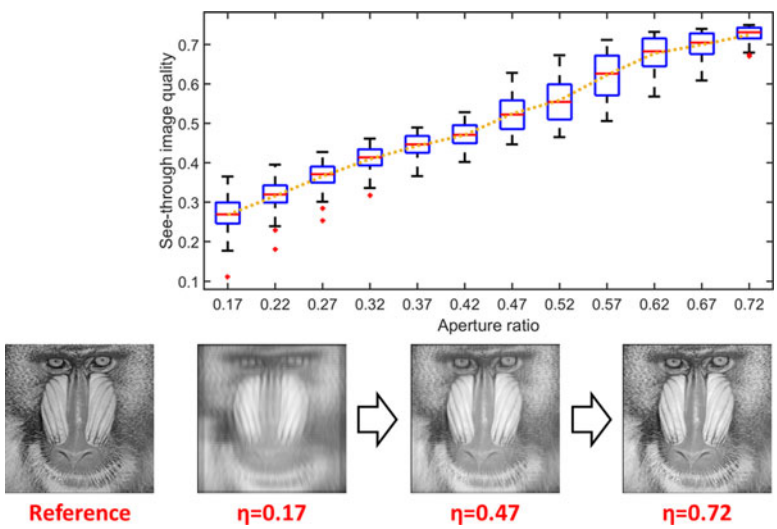

DOI: 10.1109/JPHOT.2017.2722000
1943-0655

IEEE photonics SOCIETY

IEEE

Evaluation of a Transparent Display's Pixel Structure Regarding Subjective Quality of Diffracted See-Through Images

Zong Qin,[1] Jing Xie,[2] Fang-Cheng Lin,[1] Yi-Pai Huang,[1] and Han-Ping D. Shieh,[1] *Fellow, IEEE*

[1]Department of Photonics and Display Institute, National Chiao Tung University, Hsinchu 30010, Taiwan, R.O.C.
[2]Department and Graduate Institute of Library and Information Science, National Taiwan University, Taipei 10617, Taiwan, R.O.C.

DOI:10.1109/JPHOT.2017.2722000

Manuscript received June 5, 2017; revised June 23, 2017; accepted June 27, 2017. Date of publication June 30, 2017; date of current version August 15, 2017. This work was supported by the Project of Ministry of Science and Technology, R.O.C., under Grants MOST104-2628-E-009-012-MY3, MOST105-2221-E-009-085, and MOST105-2221-E-009-086. Corresponding author: Zong Qin (e-mail: qinzong.wnlo@gmail.com).

Abstract: Transparent displays utilizing transparent windows suffer from blurred see-through images caused by diffraction; however, current studies still rely on experiments with actual display panels and human observers to investigate see-through image quality. Moreover, the influence of pixel structure on subjective see-through image quality has not been clearly demonstrated. To improve the inefficient investigation methodology and quantitatively evaluate pixel structure, we first propose a simulation method for diffracted see-through images. Next, by testing six mainstream full-reference image quality assessment algorithms, multiscale structure similarity (MS-SSIM) is revealed to be the most suitable predictor of subjective image quality for our study. Based on public image databases, the influences of aperture ratio, resolution, and the geometry of the transparent window are evaluated by combining the proposed simulation method and MS-SSIM. As a result, an aperture ratio increase of 0.1 leads to a considerable increase of subjective image quality, as more than eight percentage points. Then, a resolution increase of 100PPI only leads to an approximately three percentage point decrease of image quality. Finally, little influence of the geometry of the transparent window is demonstrated. Additionally, physical reasons why these aspects of pixel structure perform in such a manner are also given.

Index Terms: Diffractive optics, image quality assessment, pixel structure, transparent display.

1. Introduction

Transparent displays, such as transparent organic light-emitting diode (OLED) displays and liquid crystal displays (LCD), are gaining more and more attentions because they enable emerging applications, including augmented-reality devices, smart windows, vehicle head-up displays, retail showcases, *etc.* [1]–[4]. In transparent displays, displayed and see-through images are fused to be observed; thus, in addition to the displayed image quality, see-through image quality should also be of concern. Unfortunately, high-transmittance transparent displays, which utilize transparent windows to easily avoid light absorption caused by optical materials, suffer from blurred see-through images in practice [5]–[9], since the transparent window array diffracts light from ambient objects [3],

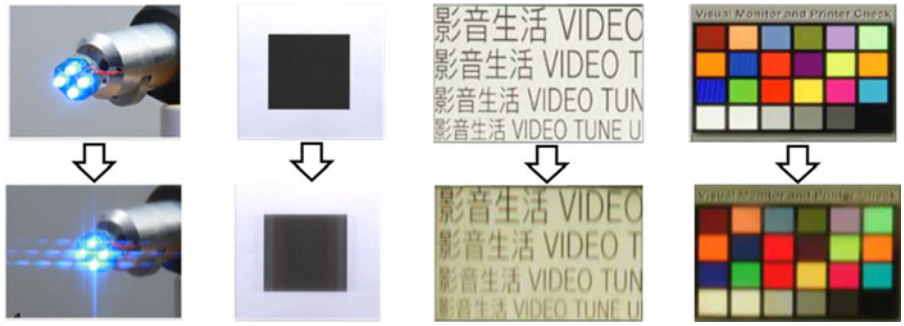

Fig. 1. Original (upper) and blurred (lower) see-through images of OLED displays.

[8]–[12]. For example, Fig. 1 demonstrates several blurred see-through images of transparent OLED displays [8], [10]–[12]. Currently, expensive and time-consuming experiments are required, along with actual display panels and human observers, to investigate see-through image quality [8]–[12]. In such experiments, observers have to determine subjective image quality by personally evaluating see-through images. To make matters worse, the pixel structure of a display is roughly and intuitively known to influence see-through image quality, whereas the exact extent of the influence is barely known. For example, if the resolution of a transparent display is doubled, the denser structure will intensify diffraction and "should" lead to lower image quality, but no study, to our knowledge, can determine whether the subjective image quality will be half or some other reduction. Therefore, to efficiently investigate the subjective see-through image quality of a transparent display that utilizes transparent windows, an evaluation methodology without actual panels or human observers is desired. Moreover, the influence of pixel structure on the image quality needs to be quantitatively demonstrated.

To solve the issues mentioned above, the following aspects are discussed in this paper. (i) First, based on diffraction theory, a calculation method is proposed to simulate a see-through image of a transparent display from the pixel structure and viewing condition, and its accuracy is experimentally verified. (ii) Next, full-reference image quality assessment (FR-IQA) is introduced from the field of image processing, and several mainstream FR-IQA algorithms are tested based on a series of see-through images. By comparing objective scores calculated by selected algorithms and subjective scores provided by a number of human observers, multiscale structure similarity (MS-SSIM) is revealed to be the most suitable predictor of subjective image quality. (iii) Based on public image databases, diffracted see-through images corresponding to different aperture ratios, resolutions, and geometries of transparent windows are simulated with the proposed method, and then, their subjective image qualities are assessed by MS-SSIM to quantitatively investigate the influences of these aspects of pixel structure.

2. Simulation of Diffracted See-Through Image

2.1. Simulation Method

The architecture in which a see-through image of a transparent display is perceived usually includes an ambient object, a transparent display panel, and a receiver containing a lens (such as a camera or human eyes), as illustrated in Fig. 2(a) and (b). In this architecture, the transparent window array diffracts light from the ambient object, and then, the receiver's lens, with aperture size D_L and focal length f, converges the light and forms an image on the focal plane, which is the human retina or a camera's sensor. Here, we define background distance (ambient object to display) and viewing distance (display to aperture of the receiver's lens) as D_1 and D_2, respectively. For experimental verification, we also construct such an architecture by placing an ambient object in a light box illuminated by a D65 source, as shown in Fig. 2(c). A Canon 5D Mark II camera with a 50 mm/F1.2 lens is used for capture through the display panel. Here, the transparent display provided by ITRI,

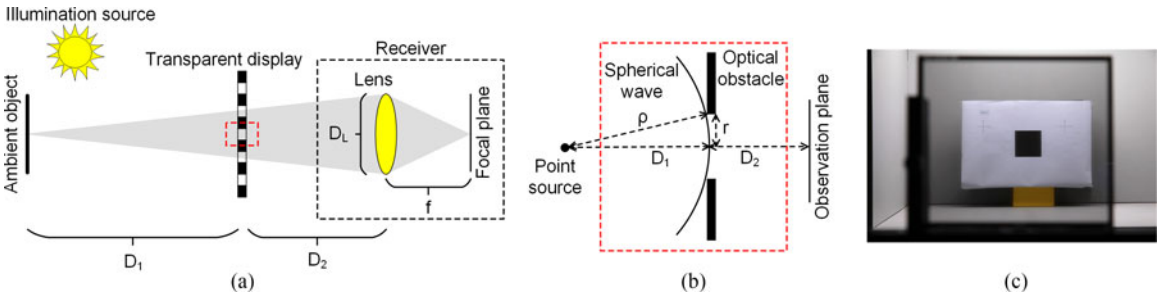

Fig. 2. (a) Architecture in which the see-through image of a transparent display is perceived, and the region around transparent windows in the red block is enlarged in (b). (c) Ambient object placed in a light box and captured by a camera through a transparent OLED display.

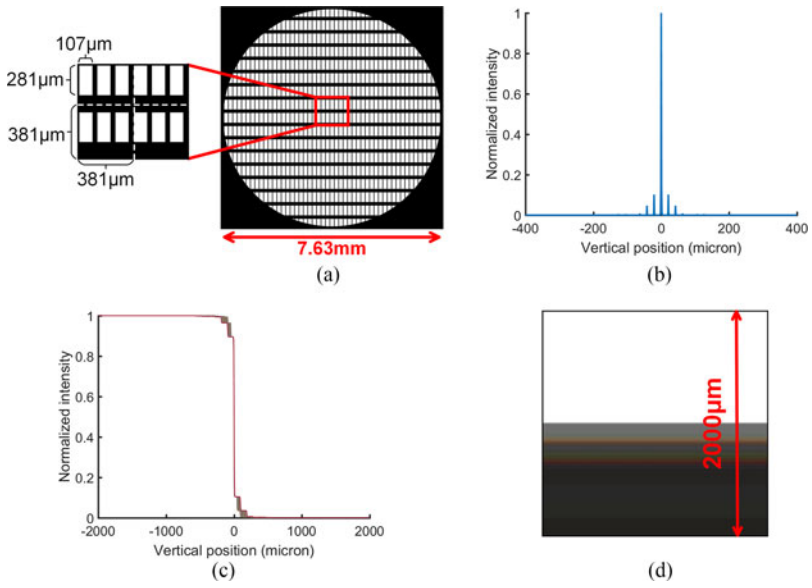

Fig. 3. (a) Display region involved in diffraction calculation, and enlarged pixel structure where white regions denote transparent windows. (b) Vertical PSF corresponding to λ of 780 nm. (c) Monochromatic diffracted see-through images of a knife edge in the vertical direction, where different lines denote different wavelengths from 380 to 780 nm. (d) Synthesized chromatic see-through image.

Taiwan is a 7 inch top-emission type active-matrix OLED display utilizing transparent windows and opaque OLED pixels. The resolution of the display is 67PPI, and each pixel contains three transparent windows corresponding to three subpixels, as shown in Fig. 3(a).

According to the schematic in Fig. 2(a), the region on the display panel involved in diffraction is approximately a circle with a diameter of $D_L \times D_1/(D_1 + D_2)$. For example, we set $D_1 = 180\,\text{cm}$, $D_2 = 30\,\text{cm}$, and $D_L = 8.9\,\text{mm}$ ($f = 50\,\text{mm}$ and $\text{F} - \text{number} = 5.6$), and then, the relevant display region can be drawn in Fig. 3(a), which is just the complex aperture function $\hat{A}(x_A, y_A)$ for the following calculations. If the incident wave-front on the display is uniform and planar, the complex amplitude distribution $\hat{H}(x_H, y_H)$ on the front surface of the receiver's lens is a Fresnel diffraction pattern of the aperture function $\hat{A}(x_A, y_A)$, as given by Eq. (1) [13]. However, the wave-front on the display panel produced by a finitely far ambient object is actually spherical, not planar. For this case, previous studies [14]–[16] validated that in the Fresnel or even nearer region, the diffraction pattern produced by a spherical wave-front shrinks from that produced by a planar wave-front with a magnification M. The value of M equals the plane-wave-case Fresnel number, **FN**, divided by the spherical-wave-case Fresnel number **FN'**. As in Fig. 2(b), **FN** can be easily obtained with the basic

definition $r^2/\lambda D_2$, where λ is wavelength, and **FN'** can be solved with Eq. (2) [16]. When the incident beam on the display is faster than *f*/12 and the *f*-number of a beam is defined as 0.5/tan[arctan(r/ρ)], **FN'** can be approximately given by Eq. (3), where **FN** is also given. Considering that the ambient object is usually not placed so close to the display panel, D_1 can always meet $\rho \approx D_1$ and *f*-number > 12. Consequently, the magnification M can be simplified to $D_1/(D_1 + D_2)$ [11]. Next, $\hat{H}(x_H, y_H)$ shrinks with magnification M and is modulated by the optical transfer function of the lens, which then produces the Fresnel diffraction pattern $\hat{S}(x_S, y_S)$ on the focal plane. According to the well-known Fourier transforming property of a thin lens [13], $\hat{S}(x_S, y_S)$ is the spatial frequency spectrum of $\hat{A}(x_A, y_A)$ multiplied by a phase shift and then shrunk with magnification M. Finally, the intensity distribution $S(x_S, y_S)$ on the focal plane, *a.k.a.* the point spread function (PSF) captured by a camera or human eyes, can finally be obtained by Fourier transforming to $\hat{A}(x_A, y_A)$, calculating the modulus square, and shrinking with magnification M, as given by Eq. (4). The calculation of PSF can be conveniently implemented in a computer by drawing the pixel structure as an image file and utilizing two-dimensional fast Fourier transformation [17], [18]. When λ is 780 nm, Fig. 2(b) demonstrates the PSF of the aforementioned example in the vertical direction, where several maxima can be found. Similarly, the PSFs of different wavelengths can be calculated.

$$\hat{H}(x_H, y_H) = \Delta\varphi_1 \cdot \exp\left[\frac{i\pi}{\lambda D_2}\left(x_H^2 + y_H^2\right)\right] \cdot \mathcal{F}\left\{\hat{A}(x_A, y_A)\exp\left[\frac{i\pi}{\lambda D_2}\left(x_A^2 + y_A^2\right)\right]\right\} \tag{1}$$

$$\frac{\lambda^2}{4(\rho + D_2)}\mathbf{FN}'^2 + \frac{\lambda z'}{\rho + D_2}\mathbf{FN}' = 2\rho\left[1 - \left(1 - \frac{r^2}{\rho^2}\right)^{1/2}\right] \tag{2}$$

$$\mathbf{FN}' = \frac{r^2}{\lambda}\left(\frac{1}{\rho} + \frac{1}{D_2}\right), \quad \mathbf{FN} = \frac{r^2}{\lambda D_2} \tag{3}$$

$$S(x_S, y_S) = |\mathcal{F}[\hat{A}(x_A, y_A)] \cdot \Delta\varphi_2|_{u=\frac{x_S/M}{\lambda f}, v=\frac{y_S/M}{\lambda f}}|^2 = |\mathcal{F}[\hat{A}(x_A, y_A)]|_{u=\frac{x_S/M}{\lambda f}, v=\frac{y_S/M}{\lambda f}}|^2 \tag{4}$$

where $\mathcal{F}$ denotes the Fourier transform; $\Delta\varphi_1$ and $\Delta\varphi_2$ are certain phase shifts; u and v are intermediate variables of frequency in the Fourier transformation; and the subscripts A, H, and S denote the coordinate system on the display panel, the front surface of the receiver's lens, and the focal plane, respectively.

With the aid of PSF, diffracted image of a point source, such as an LED light, can be obtained [8]. Nevertheless, in practical applications, arbitrary objects are desired to be investigated in addition to a point source. When the display panel is viewed on-axis, the paraxial approximation is established around the observer's sight line. In this case, our system can be regarded as spatially invariant. Thus, the calculation for one point on the ambient object, i.e., the PSF, can be spatially extended by convolution. Since the ambient object is actually formed by numerous incoherent sources, the convolution should be implemented in the term of intensity (PSF) rather than complex amplitude. For example, a lateral knife edge is adopted as the ambient object, and wavelengths from 380 to 780 nm with a step of 20 nm, are considered. By convoluting the ideal image of the knife edge with PSFs of these wavelengths, a series of monochromatic diffracted see-through images can be calculated, whose vertical distributions are shown in Fig. 3(c). Next, using the reflected spectrum over the wavelength as weighting coefficients, these monochromatic diffracted see-through images can be combined to form a color image. In this example, the reflective spectrum of the ambient object is assumed to be uniform to the D65 source, and then, XYZ tristimulus values are calculated using the photopic luminous efficiency function [19]. Finally, RGB values are converted from XYZ values by using the D65 source as a reference white for each pixel, and the synthesized color image is shown in Fig. 3(d). The transparent window array causes an apparent diffraction pattern.

In summary, the proposed simulation method for a see-through image of a transparent display requires four steps. (i) Calculate PSFs by implementing Fourier transformation on the aperture function determined by involved pixels for different wavelengths. (ii) Shrink the PSFs according to background and viewing distances. (iii) Convolute the PSFs and ideal image of the ambient

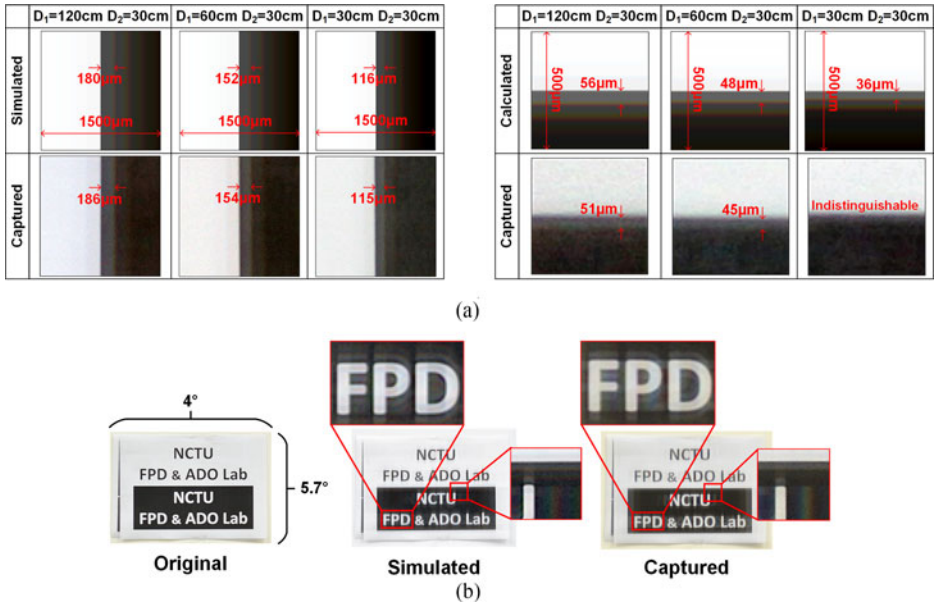

Fig. 4. (a) Simulated and captured see-through images of vertical and lateral knife edges corresponding to three background distances. Fringe lengths are marked. (b) Simulated and captured see-through images of a piece of A4 paper with some letters.

object to obtain monochromatic images for different wavelengths. (iv) Synthesize monochromatic diffracted see-through images into a chromatic image based on the luminous efficiency function and the illumination source used.

2.2. Experimental Verification

To verify the accuracy of the proposed simulation method, a transparent OLED panel, whose pixel structure is shown in Fig. 3(a), and a black square on a piece of white paper are adopted to establish the experiments, as shown in Fig. 2(c). Considering normal viewing conditions, the viewing distance D_2 is fixed at 30 cm, and three background distances D_1 of 120, 60 and 30 cm are adopted in the experiments. See-through images of the vertical and lateral knife edges are simultaneously simulated and captured (F-number: 5.6, shutter speed: 1/80 s). Fig. 4(a) demonstrates the calculated and captured images, where highly matched images can be observed. Additionally, the lengths of diffraction fringes are also marked in Fig. 4(a) and the average error rate between captured and simulated images is as low as 4.1% in terms of fringe length. Here the fringe length of the last lateral edge is too small to be resolved by our camera, i.e., the aberration of the camera dominates rather than the diffraction; hence we do not consider this indistinguishable case exceeding our capturing ability. Such a small error rate quantitatively verifies the proposed simulation method. Furthermore, a more complicated object is adopted: a piece of A4 paper with some letters. By fixing D_1 and D_2 at 270 and 30 cm, respectively, the see-through image is also simultaneously simulated and captured, as shown in Fig. 4(b). Highly matched images can also be observed, especially via enlarged details, which also verifies the proposed simulation method. More details about the verification of this simulation method can be found in [11].

3. Subjective Quality Assessment of See-Through Images

Now, we can directly use the pixel structure and viewing condition of a transparent display to accurately simulate a blurred see-through image, i.e., to remove actual display panels. Nevertheless,

since such image blurring caused by a transparent window array is quite different from that caused by regular optical aberrations, it is not apparent how to assess image quality, especially when the subjectivity of human observers should be linearly reflected [11]. Here, for this purpose, image quality assessment (IQA) that has been developed for many years in the field of image processing is introduced [20]–[28]. IQA automatically computes an objective score for the quality of a distorted image to match the subjective score of human observers. IQA can be categorized into three types [20], including full-reference IQA (FR-IQA), which calls for both the distorted image and its reference (distortion-free) image, no-reference IQA (NR-IQA), which only requires the distorted image, and reduced-reference IQA (RR-IQA), which needs the distorted image and part of its reference image. Of these three types of IQA, FR-IQA has the best prediction performance of subjective image quality because the most information is provided [20]. Fortunately, in our study, the distortion-free image of an ambient object can be easily obtained, as long as the transparent display is not applied. Therefore, FR-IQA can be utilized here with excellent performance. Due to complicated physiological-psychology mechanisms of the human vision system and diversiform types of image distortion, a single FR-IQA algorithm is hardly suitable for all images and distortion types [20]. Therefore, different FR-IQA algorithms have been proposed, which have respective superiorities based on different mechanisms [21]–[26]. To determine the most suitable algorithm for our task of assessing see-through images, four steps are needed. (i) Select several mainstream FR-IQA algorithms as candidates. (ii) Generate a series of see-through images with different pixel structures or viewing conditions. (iii) Implement human factor tests to acquire mean opinion scores (MOSs) of these see-through images. (iv) Compute objective scores of these images with candidate algorithms, compare these scores with the MOSs acquired earlier, and then, select the algorithm with the highest correlation between objective and subjective scores.

3.1. Adoption of FR-IQA Algorithms

Five mainstream FR-IQA algorithms varying with the human vision theory adopted are selected as candidates. (i) Visual saliency based index (VSI) [21]: employ a visual saliency map to extract salient image contents that are assumed to attract the most attention of the human vision system. (ii) Universal image quality index (UQI) [22], [23]: employ a combination of correlation loss, luminance distortion, and contrast distortion. (iii) Structural similarity (SSIM) [24]: extend UQI by modifying correlation, luminance, and contrast measurements to extract structural information. (iv) Multiscale SSIM (MS-SSIM) [25]: multiscale version of SSIM, which supplies more flexibility than the single-scale one in incorporating the variations of viewing conditions. (v) Feature similarity index (FSIM) [26]: employ phase congruency to extract low-level features, which are assumed to be crucial for the human vision system to understand an image, and consider gradient magnitude. Moreover, the simplest peak signal-to-noise ratio (PSNR) is also considered in comparisons. More implementation details of the mentioned algorithms can be found in [21]–[26]. To facilitate direct and linear FR-IQA algorithm predictions of MOSs, image databases established by scientific communities are needed to obtain a nonlinear fitting curve mapping initial objective scores to MOSs [27], [28]. Such image databases contain dozens of reference images and numerous distorted images with different distortion types, which further provide an MOS subjectively judged by dozens of human observers for each pair of reference and distorted images. In this way, a nonlinear fitting curve, which is usually a logistics function with five fitting parameters $P_1 \sim P_5$, given in Eq. (5) [20], can be determined. Additionally, the Pearson linear correlation coefficient (PLCC) can be calculated between mapped objective scores and MOSs to evaluate the performance of the FR-IQA algorithm. Among several public image databases, TID2013 has 3000 distorted images and is known to be the most comprehensive [27]; hence, it is adopted in this paper. Fig. 5 demonstrates the assessment results of all the distorted images in the TID2013 database versus the calculated MOSs, as well as the corresponding fitting curves and PLCCs. PSNR has a very poor performance, as expected, because the PLCC is smaller than 0.6. UQI does not perform well either. Other algorithms have quite good prediction ability, with PLCCs approximately 0.8 or even close to 0.9. Such performances

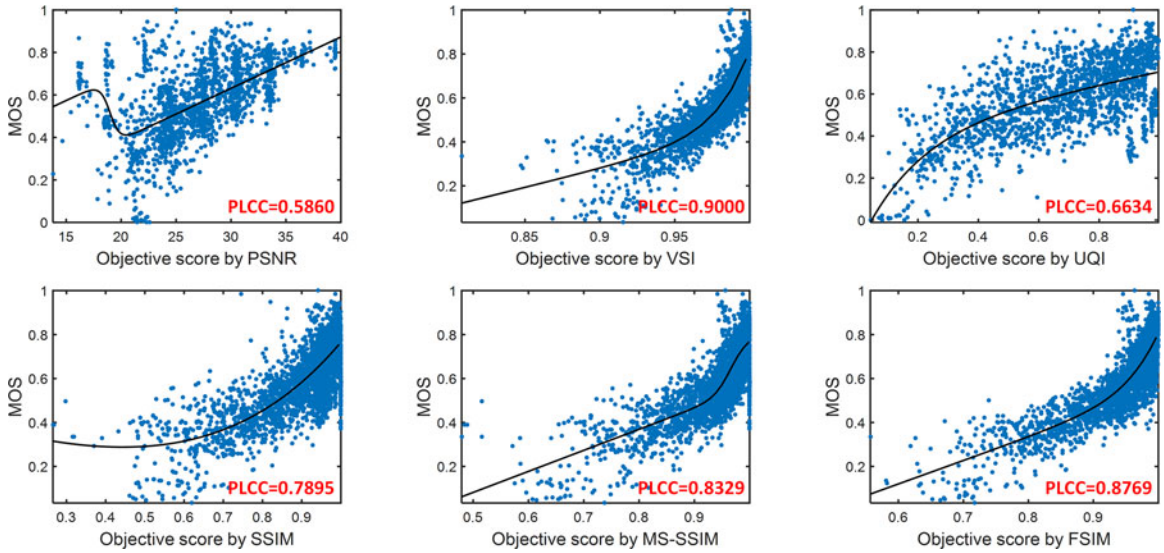

Fig. 5. Assessment results of all distorted images in the TID2013 database versus MOSs (blue points) corresponding to six candidate FR-IQA algorithms. Fitting curves (black curves) and PLCC values are also given for each algorithm.

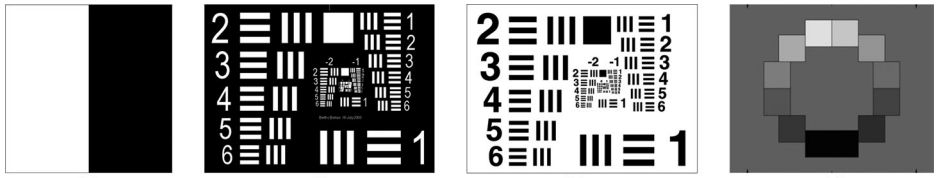

Fig. 6. (a) Knife edge; (b) black 1951 USAF chart; (c) white 1951 USAF chart; and (d) ISO-14524 chart.

are only based on general image databases. Special see-through images require the subsequent investigations.

$$I(x) = P_1 \cdot \left[0.5 - \frac{1}{1 + \exp[P_2(x - P_3)]}\right] + P_4 x + P_5 \tag{5}$$

3.2. Generation of Diffracted See-Through Images

To generate a series of see-through images with various distortion types, four typical ambient objects, including a knife edge, two high-contrast 1951 USAF charts (black and white), and a low-contrast ISO-14524 chart, are adopted as reference images and shown in Fig. 6. Here, all ambient objects are assumed to have a reflective spectrum uniform to the D65 source; therefore, weighting coefficients in the diffraction calculation can be obtained for different wavelengths.

Next, we need to set a series of parameters, including magnification $M = D_1/(D_1 + D_2)$, aperture ratio η, and resolution γ, to generate diffracted images with different distortion types. Table 1 demonstrates the setup of 43 combinations of parameters in three groups for each ambient object. In each group, one parameter varies while the other two remain invariable. Variations of aperture ratio and resolution are based on the pixel structure shown in Fig. 3(a). In this way, 43 see-through images corresponding to the 43 combinations of parameters are simulated by moving ambient objects to cover the horizontal field of view of the 50 mm lens. Finally, 172 images are generated for the four ambient objects.

TABLE 1
Parameter Combinations for Generating a Series of See-Through Images

Variable	Invariable	Minimum	Maximum	Step	Amount
Magnification M	$\eta = 0.62$, $\gamma = 67$PPI	0.05	1.00	0.05	20
Aperture ratio η	M $= 0.9$, $\gamma = 67$PPI	0.17	0.72	0.05	12
Resolution γ (PPI)	M $= 0.9$, $\eta = 0.62$	44	133	8.9	11

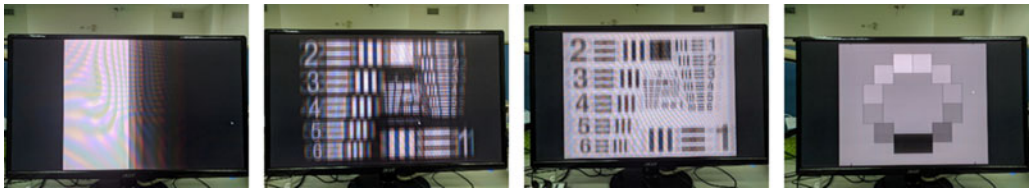

Fig. 7. Display showing test images of four different ambient objects.

3.3. Human Factor Tests

A 24-inch display is used to show test images. To reproduce the same viewing conditions as those used in see-through image simulations, images are shown in full-screen mode, and the viewing distance is 738 mm. This ensures that the field of view is the same as that of the 50 mm lens, as shown in Fig. 7. Twelve observers, aged 24 to 42, including eight males and four females, are invited. For each ambient object, observers are randomly provided with one of the 43 distorted images, following the reference image, one by one. They are asked to carefully compare the distorted and reference images and provide a quality score from 1 to 10. Between every two test periods of two objects, the observers have a one-hour rest. For each distorted image, the normalized mean value of the 12 observers' scores is determined as the MOS.

3.4. Determination of the Most Suitable FR-IQA Algorithm

Since we have acquired MOSs for 172 diffracted see-though images and introduced six candidate FR-IQA algorithms along with their implementations, the relationship between the objective scores of the 172 distorted images assessed by the candidate algorithms, and the MOSs can be determined, as shown in Fig. 8. Moreover, for the six candidate algorithms, the PLCCs between objective scores and MOSs are given in Table 2, where the PLCCs corresponding to each single ambient object and all the distorted images are given separately. PSNR has the poorest performance, as expected. VSI, UQI, and FSIM have good linear correlation for a single ambient object (PLCC close to 0.9), but they degrade severely when all images are blended (PLCC < 0.6). SSIM and MS-SSIM also have quite a good linear correlation for a single object; furthermore, SSIM has a fair overall PLCC of 0.6816, and the improved version, MS-SSIM, boosts an overall PLCC of 0.8694, which is as good as state-of-the-art FR-IQA algorithms on general image databases [20]–[26]. Therefore, MS-SSIM is determined to be the most suitable algorithm for diffracted see-through images of transparent displays.

In fact, these results are expected. Diffraction caused by a transparent window array is a type of multi-aperture diffraction, which is known to be a single aperture factor modulated by an array factor, such as that illustrated in Fig. 9 [13]. From Fig. 9, the PSF of such a diffraction features several maxima, including 0, $+1$, -1, and some insignificant higher order ones. Moreover, non-zero

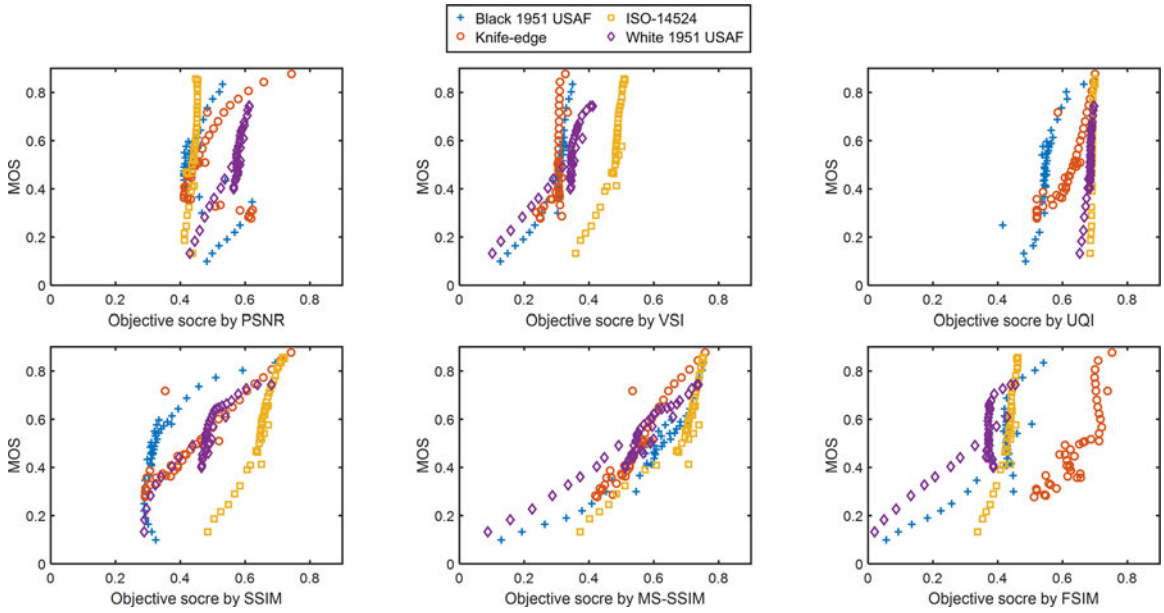

Fig. 8. Relationship between objective scores of 172 diffracted see-though images assessed by six candidate FR-IQA algorithms and MOSs.

TABLE 2
PLCC Performances of Candidate Algorithms

Ambient object	PSNR	VSI	UQI	SSIM	**MS-SSIM**	FSIM
Knife edge	0.3272	0.5668	0.8683	0.9348	**0.9526**	0.8437
Black 1951 USAF	−0.2912	0.8679	0.8346	0.7256	**0.9311**	0.8269
White 1951 USAF	0.9106	0.8993	0.9216	0.9313	**0.9536**	0.8376
ISO-14524	0.8584	0.8996	0.8868	0.9540	**0.8907**	0.9237
Overall	0.1405	0.5802	0.4716	0.6816	**0.8694**	0.3922

Bold denotes selected algorithm with the best performance.

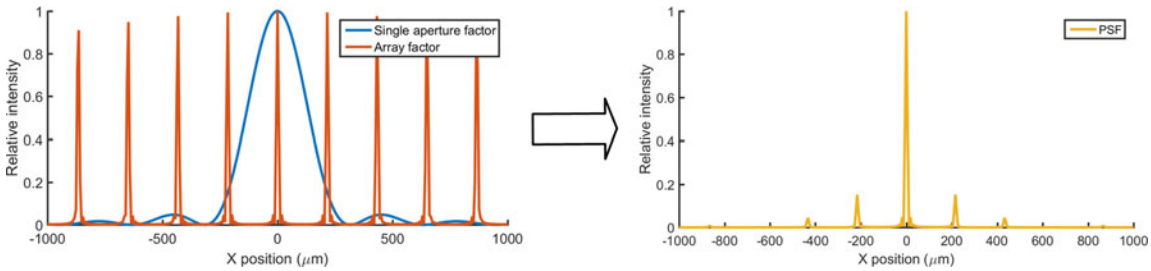

Fig. 9. The PSF of multi-aperture diffraction is actually a single aperture factor modulated by an array factor.

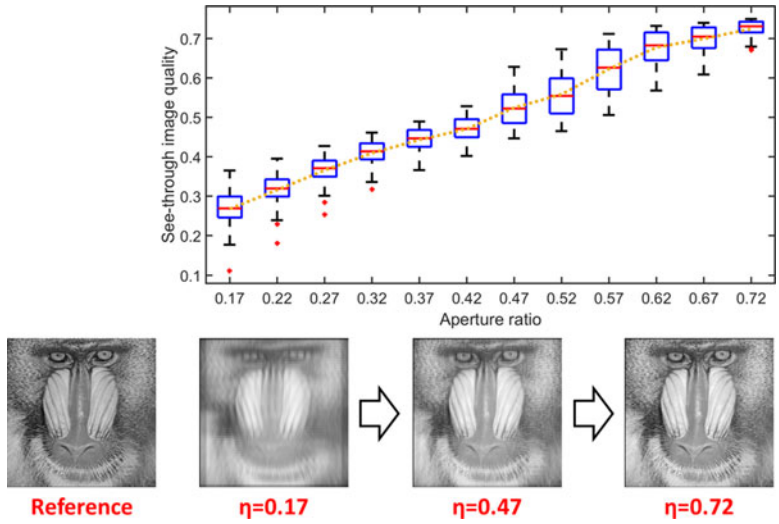

Fig. 10. Boxplot showing image quality (predicted MOS) varying with aperture ratio and distorted "Mandrill" corresponding to three different aperture ratios.

order maxima duplicate and shift original image contents to add extra structures to the image, which is where see-through image blurring essentially comes from. Since such a type of image distortion caused by extra structures is quite different from regular ones (noise, contrast shift, lens blurring, *etc.*) in general image databases, only structure-based algorithms (SSIM and MS-SSIM) can maintain performance; VSI, UQI, and FSIM, which are successful with general databases, fail here. Further, MS-SSIM is certainly better than SSIM, as it is an improved version of SSIM. Additionally, the pixel structure determines the positions and intensities of non-zero order maxima in the PSF and further determines the shift distance and brightness of duplicated image contents. In particular, the shift distance is completely dependent on the arrangement of the transparent window array, and the brightness depends on the relationship between the shape of a single window and the array arrangement. This is the manner in which pixel structure influences see-through image quality. In the following discussion of the influences of pixel structures, in addition to quantitative analysis based on FR-IQA, qualitative analysis will also be described to analyze shift distance and brightness of duplicated image contents.

4. Pixel Structure Evaluation

In the studies above, we have developed an accurate simulation method for see-though images and an effective MOS predictor, MS-SSIM. The pixel structure can be quantitatively evaluated using these two tools. Additionally, see-through image quality may vary with image contents, even if the same pixel structure is used. For example, in Fig. 8, the same parameters are applied for each reference image, whereas image quality still varies with image contents. Therefore, a variety of image contents must be included to make our pixel structure evaluation comprehensive and practical rather than just analyzing some particular images, such as a point, a knife-edge, a patch *etc*. To this end, databases TID2013 and WIQ respectively containing 25 and 7 reference images [27], [28], are adopted to include various image contents. For each pixel structure to be evaluated, the image quality scores of all 32 images are calculated by MS-SSIM and shown via boxplots in the following discussions.

4.1. Aperture Ratio

First, the background distance D_1 is 270 cm, and the viewing distance D_2 is 30 cm. The image quality (predicted MOS) varying with the aperture ratio is shown in Fig. 10 when shrinking or dilating

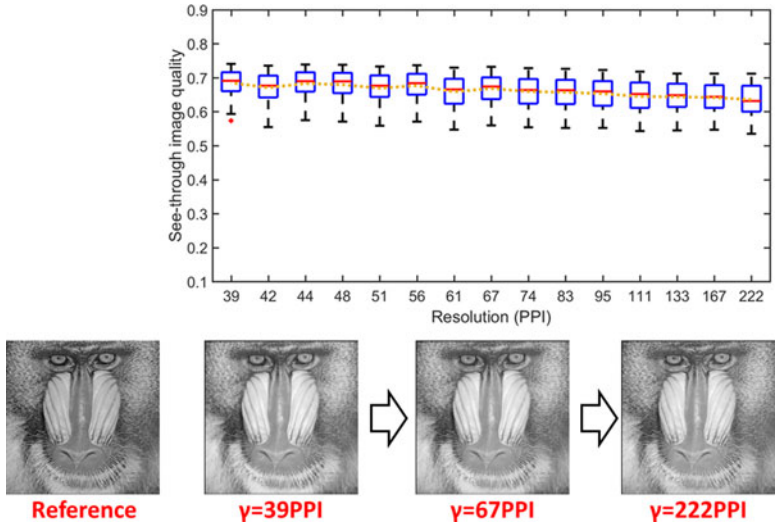

Fig. 11. Boxplot showing image quality (predicted MOS) varying with resolution, and distorted "Mandrill" corresponding to three different resolutions.

the transparent windows in the pixel structure in Fig. 3(a) and maintaining a resolution of 67PPI. The *p*-value from the correlation analysis of image quality and aperture ratio is smaller than 0.001, and the correlation coefficient is as high as 0.9973, indicating a significant linear correlation. Moreover, by implementing linear regression, the variation rate of image quality with respect to aperture ratio is 0.848, which indicates that an aperture ratio increase of 0.1 generates a more than eight percentage point increase in image quality. Therefore, a significant influence of aperture ratio on see-through image quality is demonstrated.

In this analysis, the arrangement of the transparent window array is not changed due to the constant resolution; therefore, variation of the aperture ratio only changes the brightness of duplicated image contents, without affecting the shift distance. In this way, when the aperture ratio increases, the lower brightness of duplicated content directly enhances the image quality, as intuitively shown by the famous "Mandrill" images from the WIQ database in Fig. 10.

4.2. Resolution

Similarly, D_1 is 270 cm and D_2 is 30 cm. By shrinking or dilating the whole pixel in Fig. 3(a) while keeping the aperture ratio at 0.62, resolution from 39PPI to 222PPI is evaluated. Noticeably, it is hard to achieve high transparency (aperture ratio) and high resolution simultaneously for practical transparent displays with current technologies, meaning that a panel with an aperture ratio of 0.62 and resolution of 222PPI may be unpractical. Nevertheless, to reasonably demonstrate the influence of resolution without being affected by aperture ratio variation, the value of aperture ratio is fixed at 0.62 throughout the analysis of resolution here. In addition, the transparency of high resolution transparent displays keeps increasing nowadays. In this way, once certain advanced fabrication technology can realize a high aperture ratio at high resolution someday, the evaluation results here will be valuable for the future panels immediately. Anyhow, Fig. 11 shows the evaluation results of different resolutions. Though fairly strong linear correlation is indicated by a p-value smaller than 0.001 in correlation analysis and a correlation coefficient of -0.883, the variation rate of image quality with respect to resolution obtained via linear regression is only -0.0003; that is, a resolution increase of 100PPI only leads to a three percentage point decrease in image quality. Therefore, the influence of resolution on see-through image quality is much more trivial than that of the aperture ratio.

In this case, resolution variation scales up or down the PSF to produce different shift distances of duplicated image contents, while the brightness is maintained because the relationship between

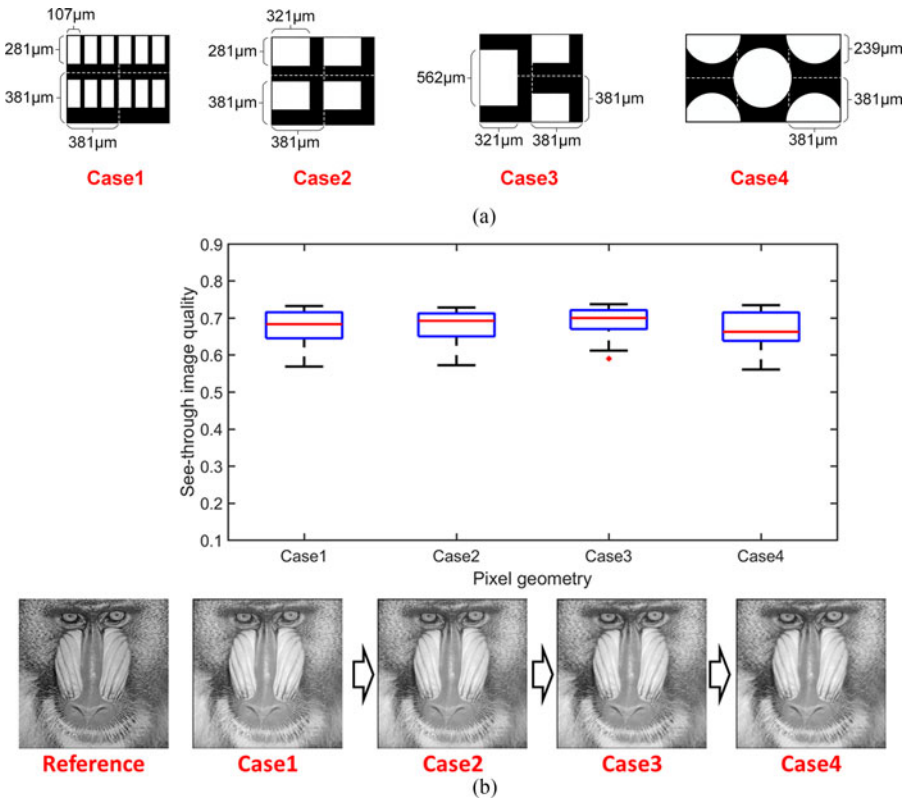

Fig. 12. (a) Pixel structures corresponding to the geometries of the four transparent windows investigated; (b) boxplot showing image quality (predicted MOS) varying with the geometry of the transparent windows, and a distorted "Mandrill" corresponding to the four different geometries.

the shape of a single window and the array arrangement does not change. A shorter shift distance caused by lower resolution appeals to the human vision system; however, it simultaneously blends original image details with duplicated contents. Thus, high-frequency image details are blurred, and the influence of a shorter shift distance is somewhat neutralized. For instance, in Fig. 11, the qualities of "Mandrill" corresponding to 39PPI, 67PPI, and 222PPI are quite close. By intuition, resolution variation directly aggravates or alleviates the diffraction, so it "should" significantly influence see-through image quality [8], [9]. Nevertheless, based on our quantitative and qualitative analyses, this concept is not correct.

4.3. Geometry of the Transparent Window

Similarly, D_1 is 270 cm and D_2 is 30 cm. The geometries of four transparent windows, including the one investigated in Fig. 3(a), with the same aperture ratio of 0.62 and resolution of 67PPI are evaluated. Fig. 12(a) and (b), respectively, demonstrates the detailed pixel structures (marked as Case1 to Case4) and see-through image qualities. According to one-way analysis of variance (ANOVA), the *p*-value is 0.147, indicating that we should reject the hypothesis that there are significant differences among the image qualities of different window geometries. In fact, by observing distorted "Mandrill" images corresponding to Case1 to Case4 in Fig. 12(b), it is difficult to subjectively differentiate their qualities.

Qualitatively, from Case1 to Case2, the increase of the lateral window size indeed alleviates diffraction in the lateral direction. However, a regular image randomly contains structures in all directions; therefore, improvement in only single direction is negligible. Furthermore, from Case2 to Case4, interlacing transparent windows or changing the geometry with equal area modifies the

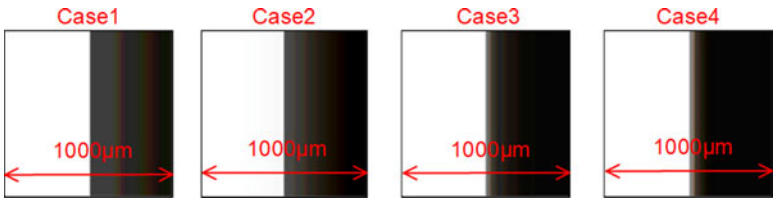

Fig. 13. See through images of a vertical knife edge produced by pixel structures Case1 to Case4.

allocation of shift distance and brightness of duplicated image contents in different spatial directions. Similarly, regular images with structures distributing in all directions result in different allocation manners performing nearly the same. Some current studies are trying to modify the geometry of the transparent window to enhance see-through image quality and have acquired some positive results [8]–[10], which seems to be inconsistent with our results. However, those studies only used particular images with image structures of limited directions, such as a knife edge, a patch, and letters, to verify performance. Specifically, Fig. 13 shows four see-through images of a vertical knife edge produced by Case1 to Case4, which were discussed in [10] and [11]. Case2 brings about a better image quality than Case1 does for a knife edge; Case3 and Case4 further lead the quality to be much better, which is naturally because of the lateral aperture function alleviating the diffraction more and more. However, such a performance cannot be validated using regular images with random image structures, for instance, the "Mandrill" in Fig. 12. Finally, our study demonstrates that modifying the geometry of the transparent window does not improve see-through image quality.

5. Conclusions

In this paper, we sought to efficiently investigate the see-through image quality of a transparent display using transparent windows and then quantitatively evaluate the pixel structure regarding subjective see-through image quality. Therefore, we proposed a simulation method for see-through images based on diffraction theory, and revealed that MS-SSIM is the most suitable FR-IQA algorithm to assess the subjective quality of diffracted see-through images. Based on the proposed simulation method and MS-SSIM, three aspects of pixel structure, including aperture ratio, resolution, and the geometry of the transparent window, were quantitatively evaluated. As a result, the aperture ratio significantly influences see-through image quality: an aperture ratio increase of 0.1 leads to an increase of more than eight percentage points in subjective image quality. The influence of resolution was demonstrated to be much more trivial: a resolution increase of 100PPI only leads to a decrease of three percentage points of subjective image quality. Finally, the geometry of the transparent window hardly influences see-through image quality, which indicates that modifying the window geometry is fruitless. The physical essentials of these performances were also qualitatively explained based on multi-aperture diffraction theory.

In conclusion, this paper proposed an efficient evaluation method for pixel structure regarding subjective see-through image quality and also provided useful guidelines for pixel structure design by demonstrating quantitative influences of different aspects of the pixel structure, especially demonstrating that resolution and window geometry deserve less attention than common intuition expects. Therefore, when utilizing transparent displays to realize augmented-reality head-mounted display, vehicle head-up display, smart windows, *etc.*, this study can be a reference for assessing the see-through image to obtain a high quality display device.

References

[1] M. Bergman, "Product and technology trends from the 2015 International CES," *IEEE Consum. Electron. Mag.*, vol. 4, no. 3, pp. 99–100, Jul. 2015.
[2] D. C. Choe, G. W. Kim, R. Lampande, and J. H. Kwon, "Smart window devices for black screen of organic light emitting diodes," *SID Symp. Dig. Tech. Papers*, vol. 46, no. 1, pp. 821–823, 2015.

[3] C. W. Kuo *et al.*, "Flat type transparent display demonstrating field-sequential-color," *SID Symp. Dig. Tech. Papers*, vol. 47, no. 1, pp. 168–170, 2016.
[4] J. W. Huh *et al.*, "The optical effects of capping layers on the performance of transparent organic light-emitting diodes," *IEEE Photon. J.*, vol. 4, no. 1, pp. 39–47, Feb. 2012.
[5] J. Yeon, T. W. Koh, H. Cho, J. Chung, S. Yoo, and J. B. Yoon, "Actively transparent display with enhanced legibility based on an organic light-emitting diode and a cholesteric liquid crystal blind panel," *Opt. Express*, vol. 21, no. 8, pp. 10358–10366, 2013.
[6] P. Görrn *et al.*, "Towards see-through displays: fully transparent thin-film transistors driving transparent organic light-emitting diodes," *Adv. Mater.*, vol. 18, no. 6, pp. 738–741, 2006.
[7] Y. Takaki and Y. Yamaguchi, "Flat-panel see-through three-dimensional display based on integral imaging," *Opt. Lett.*, vol. 40, no. 8, pp. 1873–1876, 2015.
[8] Y. H. Tsai, M. H. Huang, W. D. Jeng, T. W. Huang, K. L. Lo, and M. Ou-Yang, "Image quality affected by diffraction of aperture structure arrangement in transparent active-matrix organic light-emitting diode displays," *Appl. Opt.*, vol. 54, no. 28, pp. E136–E145, 2015.
[9] K. L. Lo, Y. H. Tsai, W. Y. Cheng, W. D. Jeng, and O. Y. Mang, "Late-news poster: Evaluation of image quality through the transparent display," *SID Symp. Dig. Tech. Papers*, vol. 46, no. 1, pp. 1406–1409, 2015.
[10] Z. Qin *et al.*, "See-through image blurring of transparent OLED display: Diffraction analysis and OLED pixel optimization," *SID Symp. Dig. Tech. Papers*, vol. 47, no. 1, pp. 393–396, 2016.
[11] Z. Qin, Y. H. Tsai, Y. W. Yeh, Y. P. Huang, and H. P. D. Shieh, "See-through image blurring of transparent organic light-emitting diodes display: calculation method based on diffraction and analysis of pixel structures," *J. Display Technol.*, vol. 12, no. 11, pp. 1242–1249, 2016.
[12] P. Sunhee *et al.*, "Investigation on optical performance of transparent displays," in *Proc. IEEE 4th Int. Conf. Consum. Electron.*, Berlin, 2014, pp. 343–345.
[13] J. W. Goodman, *Introduction to Fourier Optics*. Englewood, CO, USA: Roberts and Company Publishers, 2005.
[14] A. M. Steane and H. N. Rutt, "Diffraction calculations in the near field and the validity of the Fresnel approximation," *J. Opt. Soc. Amer. A*, vol. 6, no. 12, pp. 1809–1814, 1989.
[15] W. H. Southwell, "Validity of the Fresnel approximation in the near field," *J. Opt. Soc. Amer.*, vol. 71, no. 1, pp. 7–14, Jan. 1981.
[16] H. G. Kraus, "Huygens–Fresnel–Kirchhoff wave-front diffraction formulation: Spherical waves," *J. Opt. Soc. Amer. A*, vol. 6, no. 8, pp. 1196–1205, 1989.
[17] K. M. Abedin, M. R. Islam, and A. F. M. Y. Haider, "Computer simulation of Fresnel diffraction from rectangular apertures and obstacles using the Fresnel integrals approach," *Opt. Laser Technol.*, vol. 39, no. 2, pp. 237–246, 2007.
[18] J. Li, Z. Peng, and Y. Fu, "Diffraction transfer function and its calculation of classic diffraction formula," *Opt. Commun.*, vol. 280, no. 2, pp. 243–248, 2007.
[19] H. S. Fairman, M. H. Brill, and H. Hemmendinger, "How the CIE 1931 color-matching functions were derived from Wright-Guild data," *Color Res. Appl.*, vol. 22, no. 1, pp. 11–23, 1997.
[20] D. M. Chandler, "Seven challenges in image quality assessment: past, present, and future research," *ISRN Signal Process.*, vol. 2013, 2013, Art. no. 905685.
[21] L. Zhang, Y. Shen, and H. Li, "VSI: A visual saliency-induced index for perceptual image quality assessment," *IEEE Trans. Image Process.*, vol. 23, no. 10, pp. 4270–4281, Oct. 2014.
[22] W. Zhou and A. C. Bovik, "A universal image quality index," *IEEE Signal Process. Lett.*, vol. 9, no. 3, pp. 81–84, Mar. 2002.
[23] H. R. Sheikh, M. F. Sabir, and A. C. Bovik, "A statistical evaluation of recent full reference image quality assessment algorithms," *IEEE Trans. Image Process.*, vol. 15, no. 11, pp. 3440–3451, Nov. 2006.
[24] W. Zhou, A. C. Bovik, H. R. Sheikh, and E. P. Simoncelli, "Image quality assessment: From error visibility to structural similarity," *IEEE Trans. Image Process.*, vol. 13, no. 4, pp. 600–612, Apr. 2004.
[25] Z. Wang, E. P. Simoncelli, and A. C. Bovik, "Multiscale structural similarity for image quality assessment," in *Proc. 37th Asilomar Conf. Signals, Syst. Comput.*, 2003, pp. 1398–1402.
[26] L. Zhang, L. Zhang, X. Mou, and D. Zhang, "FSIM: A feature similarity index for image quality assessment," *IEEE Trans. Image Process.*, vol. 20, no. 8, pp. 2378–2386, Aug. 2011.
[27] N. Ponomarenko *et al.*, "Image database TID2013: Peculiarities, results and perspectives," *Signal Process. Image Commun.*, vol. 30, pp. 57–77, 2015.
[28] U. Engelke, M. Kusuma, H. J. Zepernick, and M. Caldera, "Reduced-reference metric design for objective perceptual quality assessment in wireless imaging," *Signal Process. Image Commun.*, vol. 24, no. 7, pp. 525–547, 2009.